Highlights

- Manganese-doped Lanthanum oxycarbonate (MnL) catalysed H_2O_2 oxidation to remove As
- The approach effectively oxidised As(III) and adsorbed As(V) over a wide pH range
- As(III) was mainly oxidised by ROSs generated from La(III) Lewis acid-base adduct
- Variously-valent Mn contributed both to catalytic ROSs generation and As adsorption
- MnL exhibited stable performance with coexisting ions and also after 3 times reuse

Graphical abstract

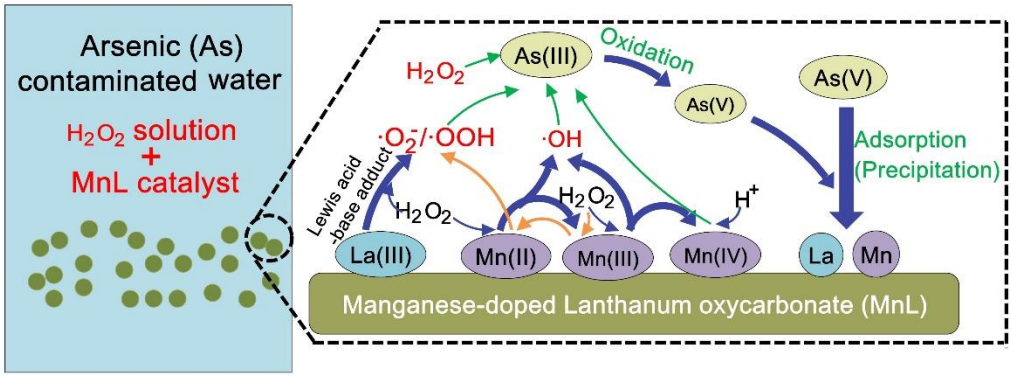

Efficient Arsenic (As) removal by manganese-doped Lanthanum oxycarbonate enabled with enhanced H_2O_2 catalytic oxidation of As(III) and adsorption of As(V)

Jing Su[a,b,c], Tao Lyu*[d], Mick Cooper[e], Robert J.G. Mortimer[f,g], Gang Pan*[a,b,e,g]

[a] *Key Laboratory of Environmental Nanotechnology and Health Effects, Research Center for Eco-Environmental Sciences, Chinese Academy of Sciences, Beijing 100085, P. R. China*

[b] *University of Chinese Academy of Sciences, Beijing 100049, P. R. China*

[c] *Institute of Technology Development, Wuhuan Engineering Co.,Ltd, Wuhan 430070, P.R.China*

[d] *Cranfield Water Science Institute, Cranfield University, College Road, Cranfield, Bedfordshire, MK43 0AL, UK*

[e] *School of Animal, Rural, and Environmental Sciences, Nottingham Trent University, Brackenhurst Campus, Nottinghamshire, NG25 0QF, UK*

f York St John University, Lord Mayor's Walk, York YO31 7EX

g Nanjing Xianglai Academy of Eco-environmental Science and Technology, Nanjing, China

* Corresponding authors: gang.pan@ntu.ac.uk (G.P.); t.lyu@cranfield.ac.uk (T.L.)

Abstract

The oxidation of arsenite (As(III)) to arsenate (As(V)) is an important approach for lowering the toxicity of As-contaminated water. However, in order to completely remediate the problem, the As(V) must also be removed. This study evaluates a novel heterogenous catalytic system using manganese-doped Lanthanum oxycarbonate (MnL) to catalyse the oxidation of As(III) by H_2O_2 and simultaneously adsorb the generated As(V). The presence of MnL enhanced the oxidation rate of As(III) by 35 times compared with systems utilising H_2O_2 alone. Additionally, this superior performance was observed over a wide pH range (5-9), which demonstrated that this approach could bypass the well-known pH restriction on oxidation by H_2O_2. Mechanistic studies revealed that the long-lived superoxide radicals ($\cdot O_2^-$/$\cdot$OOH), present on the particle surfaces and derived from the dissociation of the Lewis acid-base adduct (La-OOH*), were the dominant active species for As(III) oxidation. Mn atoms with low valence states played a crucial role on As(III) oxidation through the provision of extra active sites to facilitate radical production, and improve H_2O_2 adsorption on the MnL surface for the reaction. The La and Mn sites in MnL could thus rapidly immobilize the generated As(V) by forming precipitates, resulting in a final As removal efficiency of 99%, even after three cycles of reutilisation. These results demonstrate this process represents a promising strategy for As removal and has developed novel materials for efficient As remediation through

integrated As(III) oxidation and As(V) adsorption.

Keywords: Advanced oxidation; Adsorbent nanomaterial; Heavy metals; Lewis acid-base adduct; Reactive oxidise species (ROSs)

1. Introduction

Arsenic (As) is one of the most widespread heavy metal contaminants in both surface and groundwater systems and poses a severe risk to the aquatic environment and to human health (Argos et al. 2012, Su et al. 2018). Related human disease and mortality have been reported in many countries (Ahmad et al. 2018, Smith et al. 2012), thus the World Health Organization (WHO) has set a safety level of 10 μg L^{-1} As in drinking waters (Wei et al. 2019). In solution under anoxic and anaerobic conditions, As mainly exists as the trivalent species As(III) (Shan et al. 2019a). Since the mobility and toxicity of As(III) are substantially greater than those of As(V) (Qiu et al. 2020), the removal of As(III) from aqueous environments has drawn particular attention. Unlike As(V), As(III) shows much less affinity with adsorbents due to it mainly existing as a non-ionic molecule (H_3AsO_3) in water (Shan et al. 2019b). Therefore, the development of As(III) decontamination technology to support environmental sustainability and public health remains a significant challenge..

Hydrogen peroxide (H_2O_2) has been used as a benign oxidant to convert As(III) to less toxic As(V) in water and wastewater treatment processes (Eq. 1) due to its superior oxidation potential (Wei et al. 2019). However, the oxidative activity of H_2O_2 is strongly pH-dependent and functionality could be significantly inhibited along with the decrease of alkalinity in solution (Shan et al. 2019b). In order to broaden the applicable pH range of H_2O_2 and to increase oxidation efficiency, some catalysts are suggested to stimulate the reaction. Among them, the most common method has been to apply Fenton-like catalysts, such as Fe, Cu and Mn-based (hydro)oxides, which could act as an electron shuttle to accelerate the dissociation of H_2O_2 and produce more powerful reactive oxygen species (ROSs), e.g. ·OH and $\cdot O_2^-$ (Eq. 2-3) (Wang et al. 2015, Weng et al. 2017, Yang et al. 2019). Recently, another effective approach, using transition metal (hydro)oxides, e.g. Ti, Ce, Zn, to form Lewis-acid centres on the material surface in H_2O_2 solution during oxidation reactions, has been discovered (Chen et al. 2012, Fernandes et al. 2020, Kim et al. 2015). Such Lewis acid catalysis could complex with H_2O_2 and withdraw electrons from its O-O bond, thus leading to the generation of the strong oxidative radicals (Eq. 4), such as ·OOH, ·OH or $^1O_2$, towards facilitating As(III) oxidation (Corma and Garcı´a 2002, Wang et al. 2018). Nevertheless, simply oxidising As(III) only decreases the toxicity of the As contaminated water, and subsequent removal through adsorption, coagulation, or ion exchange is needed to remove the environmental

risk(Manning et al. 2002, Nicomel et al. 2016).

$$H_2AsO_3^- + H_2O_2 \rightarrow HAsO_4^{2-} + H^+ + H_2O \quad (1)$$

$$\equiv Fe(II) + H_2O_2 \rightarrow \equiv Fe(III) + \cdot OH + OH^- \quad (2)$$

$$\equiv Fe(III) + H_2O_2 \rightarrow \equiv Fe(II) + \cdot OOH/\cdot O_2^- + H^+ \quad (3)$$

$$\equiv Ti(IV) - OH + H_2O_2 \rightarrow \equiv Ti(III) - \cdot OOH + H_2O \quad (4)$$

We have previously synthesised a novel manganese-doped Lanthanum oxycarbonate (MnL) adsorbent and demonstrated its superior As(V) adsorption ability (555.6 mg L^{-1}) compared with that (26.3-454.9 mg L^{-1}) of other reported natural and synthesised adsorbents (Su et al. 2020). Interestingly, the Lanthanum (La) sites in this La-based compound act as Lewis acids, which have been applied as complexation agents for many anions (Muthu Prabhu et al. 2018, Wahlen et al. 2005). Thus, we hypothesized that MnL could not only adsorb As(V), but also accelerate As(III) oxidation through catalytic activity in generating ROSs by forming Lewis acid-base adducts with H_2O_2. Moreover, MnL has been demonstrated to possess a relatively stable performance for As(V) adsorption over a wide pH range of 4-9 (Su et al. 2020), which may additionally assist in overcoming the pH limit on the H_2O_2 oxidation process. Thus, the pre-treatment of As(III), which converts As(III) to As(V), followed by As(V) adsorption is an effective way to completely removal As from aqueous media (Ding et al. 2018). The application of MnL during As(III) oxidation by H_2O_2 may form a heterogenous catalytic system to fulfil the dual functions of catalysed oxidation and adsorption of the generated As(V), has hitherto not been studied.

Therefore, this study aimed to develop and evaluate a potential multi-functional catalyst for the removal of As(III) from aqueous environments through simultaneous H_2O_2 catalytic oxidation and adsorption of As(V), over a wide pH range. Firstly, the capabilities of synthesised MnL materials with different relative percentage compositions of Mn and La, on As(III) oxidation and on total removal of As in H_2O_2 solutions, were evaluated. Then, the potential effects of experimental factors, including pH conditions and the dosage of H_2O_2 and MnL on the oxidation of As(III), were investigated. Furthermore, mechanistic studies were conducted to determine the potential roles of specific reactive oxygen species on As(III) oxidation, the functionality of La and Mn lattice sites, on the overall treatment process. After understanding the mechanisms, the potential application of MnL in H_2O_2 catalytic oxidation processes was further examined in the presence of other, possibly interfering, ions and finally, reusability of the material was investigated by subjecting the catalyst to several cycles of use and regeneration, and monitoring the efficiency of As remediation.

2. Materials and Methods

2.1. Chemicals and materials

Lanthanum nitrate hexahydrate ($La(NO_3)_3 \cdot 6H_2O$,99%), hydrogen peroxide (H_2O_2, 30%), sodium arsenate dodecahydrate ($Na_3AsO_4 \cdot 12H_2O$, 99%) and sodium arsenite ($NaAsO_2$, 99%) were purchased from Aladdin Industrial Co. Ltd. (Shanghai, China). Manganese nitrate solution ($Mn(NO_3)_2$, 50%), citric acid monohydrate (AM, $C_6HO_7 \cdot H_2O$,99%), polyethene glycol 6000 (PEG-6000, 99%), ammonium molybdate ($(NH_4)_6Mo_7O_{24} \cdot 4H_2O$, 99%), ascorbic acid (AA, $C_6H_8O_6$, 99%), tertiary butanol (TBA, $C_4H_{10}O$, 99%), p-benzoquinone (p-BQ, $C_6H_4O_2$, 99%) and the spin-trapping agent 5,5 dimethyl-1-pyrroline N-oxide (DMPO, 99%) were purchased from Sinopharm Co. Ltd. (Shanghai, China). Ultrapure water (18 MΩ·cm) was used in all experiments.

2.2. Preparation and characterization of Mn-doped $La_2O_2CO_3$ (MnL)

Mn-doped $La_2O_2CO_3$ (MnL) was synthesised via a facile sol-gel method according to Su., et al. (2020). During the synthesis, the percentages of precursor $Mn(NO_3)_2/(Mn(NO_3)_2+La(NO_3)_3)$ added were 2.56%, 5.26%, 25% and 50% thus resulting in the formation of different materials. Pure $La_2O_2CO_3$ was prepared by the same process but without $Mn(NO_3)_2$ addition. The crystal structures of MnL before and after reaction were determined by X-Ray diffraction (XRD) using a PANalytical X'Pert PRO powder diffraction system (Malvern Panalytical, Cambridge, UK) with Cu Kα radiation (λ=1.5406 Å) from 5° to 90°/2θ at a scan speed of 5°/min. The morphology of the samples and their microstructure were recorded by Environmental Scanning Electron Microscope (ESEM, Su-8020, Hitachi, Japan). X-ray Photoelectron spectra (XPS; SCALAB250Xi, Thermo Fisher Scientific, USA) were collected using a monochromatic Al Kα radiation source (1486.6eV) and all binding energies were calibrated by contaminant carbon (C1s, B.E= 284.8 eV). To determine the existence of peroxide species on the material's surface, diffuse reflectance UV-visible spectra of MnL and H_2O_2-pretreated MnL was recorded using a UV-visible spectrophotometer (DR-UVS; Cary 500 UV-Vis, Varian Inc., Palo Alto, CA. USA), equipped with a diffuse reflectance accessory. Formation of surficial complexation was also investigated by Raman spectroscopy (LabRAM HR Evolution, HORIBA, France) using the excitation wavelength of 785 nm.

2.3. Experiments and sample analysis

2.3.1. The effect of MnL/H_2O_2 coupling treatment

Different MnL materials with differing contents of Mn (2.56%, 5.26%, 25% and 50%) and the pristine $LaMnO_3$ were firstly evaluated for potential catalysis of the H_2O_2 oxidation of As(III) under identical neutral conditions. The same dosage of different MnL (0.2 g L^{-1}) was added into $NaAsO_2$ solutions (60 mL) with an initial As(III) concentration of 15 mg L^{-1}. The pH was adjusted to 7 using 0.1-1 M HNO_3/NaOH. The mixture was continuously stirred in the dark and the oxidation reaction was then initiated by addition of H_2O_2 (0.534 mM). The experiment was conducted at room temperature (25 ± 2℃) for

360 min. Each treatment was carried out in triplicate.

At given time intervals along with the batch experiment, an aliquot (2.5 mL) of the suspensions were withdrawn from each group. The removed samples were then mixed with ascorbic acid (10 g L^{-1}; 200 µL) in order to quench the reactions, and filtered immediately through a cellulose acetate membrane (0.22 µm) for determination of the concentrations of total As, As(V), and As(III) remaining. The concentration of As(V) in each sample was determined colorimetrically by the molybdenum blue method (Kim et al. 2015) using a UV/visible spectrometer (870 nm; 756 PC, Hong Ji Instrument. Co., Ltd., Shanghai). For determination of total As, $KMnO_4$ solution (1 mL; 2 mM) was added into the sample to oxidise As(III) to As(V) before the detection of the latter. The concentrations of As(III) were determined by subtraction between total As and As(V). The pseudo-first-order model (Eq. 5) was used to simulate the dynamics of As(III) removal (Wang et al. 2020).

$$-\ln\left(\frac{C_t}{C_0}\right) = k_{obs}t \quad (5)$$

Where C_t was As(III) concentration (mg L^{-1}) versus time (min), C_0 was initial As(III) concentration (mg L^{-1}). k_{obs} was rate constant of the first-order kinetic (min^{-1}).

2.3.2. The effect of H_2O_2 and MnL dosage

The best-performing MnL adsorbent, containing 5.26% of Mn, was used to further investigate the influence of H_2O_2 and MnL dosage on As(III) oxidation. To study the effect of the H_2O_2, different experiments were conducted with dosages of 0.267, 0.534, 1.335, 2.67 and 5.34 mM of H_2O_2. For the investigation into MnL dosing, experiments were conducted with MnL dosages at 0.1, 0.2, 0.5 and 1 g L^{-1}. Experimental conditions and sample analysis were the same as the aforementioned batch experiment. The pseudo-first-order model (Eq. 5) was again applied to evaluate the removal rate of As(III) under the different treatments.

2.3.3. The effect of pH

The removal of As(III), As(V) and total As, were investigated under H_2O_2 oxidation only, and MnL/H_2O_2 coupling treatments under various conditions of pH (3, 5, 7, 9 and 11). The initial As(III) concentration was set at 20 mg L^{-1}, and the dosages of MnL and H_2O_2 were 0.2 g L^{-1} and 0.534 mM in the corresponding systems. The experiments were conducted at room temperature (25 ± 2℃) and sample collection and analysis were the same as previously described. The amounts of Mn^{2+} and La^{3+} liberated were detected by Inductively Coupled Plasma-Optical Emission Spectroscopy (ICP-OES; Optima 8300, Perkin Elmer Inc., USA) with a limit of detection (LOD) of 0.2 mg L^{-1}. Inductively Coupled Plasma-Mass Spectrometry (ICP-MS; 7500a, Agilent Inc., USA) was used to confirm results when concentration levels were found to be below 0.2 mg L^{-1}.

2.3.4. The role of ROSs on As(III) oxidation

During the previously-described MnL/H_2O_2 -coupled treatment at pH of 7, the ESR spectra of reactive oxygen species (·OH, and ·O_2^-/·OOH) generated were investigated using a Bruker microESR (Bruker BioSpin GmbH, Rheinstetten, Germany), using DMPO as radical trapping agent. After confirming the existence of the ROSs, the role of each on As(III) oxidation was further studied through active species trapping experiments. The performances for As removal were investigated by addition of the corresponding scavengers (Kim et al. 2015), i.e. TBA (100 mM) for ·OH and p-BQ (5 mM) for ·O_2^-/·OOH, to the mixture and the results compared with the control group without addition of the scavengers. To verify the generation of ·O_2^-/·OOH derived from the surface complex and define its effect on As(III) oxidation, diffuse reflectance UV-visible spectra (DR-UVS) and Raman spectra of MnL, before and after the treatment, were acquired.

The contribution of dissolved oxygen to the generation of ·O_2^-/·OOH and As(III) oxidation was firstly evaluated by conducting the experiment under O_2 and N_2 aeration at 5 mL min^{-1}. Experimental conditions, sample collection and analysis were the same as previously described. To further probe the role of La lattice sites on H_2O_2 dissociation and As(III) oxidation, NaF (2 mM) was added to the solution which was further stirred in the dark for 3 h to ensure La sites were completely occupied (Wu et al. 2018). H_2O_2 (0.534 mM) was then added to initiate the oxidation reaction and the oxidation performance subsequently determined.

In order to evaluate the function of Mn lattice sites on As(III) oxidation and As(V) adsorption, the different valent states of Mn (Mn(II), Mn(III) and Mn(IV)) were determined at the end of this MnL/H_2O_2 coupling treatment. For the comparison, $La_2O_2CO_3$, instead of MnL, was used in the control groups. The concentration of H_2O_2 was determined by titanium potassium oxalate spectrophotometry at 400 nm (Shan et al. 2019b). In addition, cyclic voltammetry (CV) measurements were conducted using an electrochemical work station in a standard three-electrode configuration, with N_2-purged Na_2SO_4 (50 mL, 0.5 M) containing H_2O_2 (0.534 mM) as the electrolyte (Tian et al. 2019). The MnL electrode was prepared by dispersing MnL (5 mg) in ethanol (1mL) which contained PTFE solution (50 µL; 5%), and then dried under vacuum before coating onto the pretreated FTO surface. The potential range was between −1.2 and 1.5 V (vs. Ag/AgCl) and the scan rate was 500 mV s^{-1}.

2.3.5. The reusability of MnL and the influence of coexisting ions

The regeneration of MnL was investigated by immersing the used catalysts into NaOH solution (1 M) for 24 h, to ensure that all the As(V) adsorbed on MnL had been eluted out. The refreshed material (0.2 g L^{-1}) and H_2O_2 (0.534 mM) were then added to an As(III) solution (20 mg L^{-1}), in order to evaluate the reusability of MnL. This procedure was repeated 3 times. Moreover, the effect of typical coexisting ions (Xu et al. 2020), i.e.

Fe^{3+}, Mn^{2+}, Cl^{-}, $H_2PO_4^{-}$ and HCO_3^{-}, on the As(III) oxidation process was also evaluated. MnL/H_2O_2 coupling treatments were separately conducted at initial ionic concentrations of 0, 0.2 and 2 mmol L^{-1}. After 360 min reaction time, 5 mL aliquots were collected from each group for As(III) determination. All of the aforementioned experiments and each sample analysis were conducted in triplicate.

3. Results and Discussion

3.1. Characterization of Mn-doped $La_2O_2CO_3$ (MnL) composites

The XRD patterns of the pristine $La_2O_2CO_3$ (Fig. 1a) indicated that it existed as a monoclinic structure (JCPDS card No. 48-1113). Doping of a small amount of Mn (≤5.26%) on $La_2O_2CO_3$ improved the crystal symmetry and resulted in a crystal structure similar to that of tetragonal $La_2O_2CO_3$ (JCPDS card No. 23-0320). After further increasing the amount of Mn doped into MnL to 25% and 50%, clear characteristic peaks of $LaMnO_3$ (JCPDS card No. 01-089-2470) were observed (Fig. 1a). Such a new phase of manganese oxide precipitation on the surface of $La_2O_2CO_3$ may have been due the introduction of excess Mn in its lattice cells (Xuan et al. 2018). ESEM images of MnL indicated a rod-like morphology with rod length of 1.7-4 μm (Fig. 1b-c), and element mapping of MnL suggested that both La and Mn were uniformly distributed on the material's surface (Fig. 1d-g). Characterisation confirmed that Mn atoms had successfully entered into $La_2O_2CO_3$ lattices, giving rise to the formation of La-Mn solid solution (Wang et al. 2018).

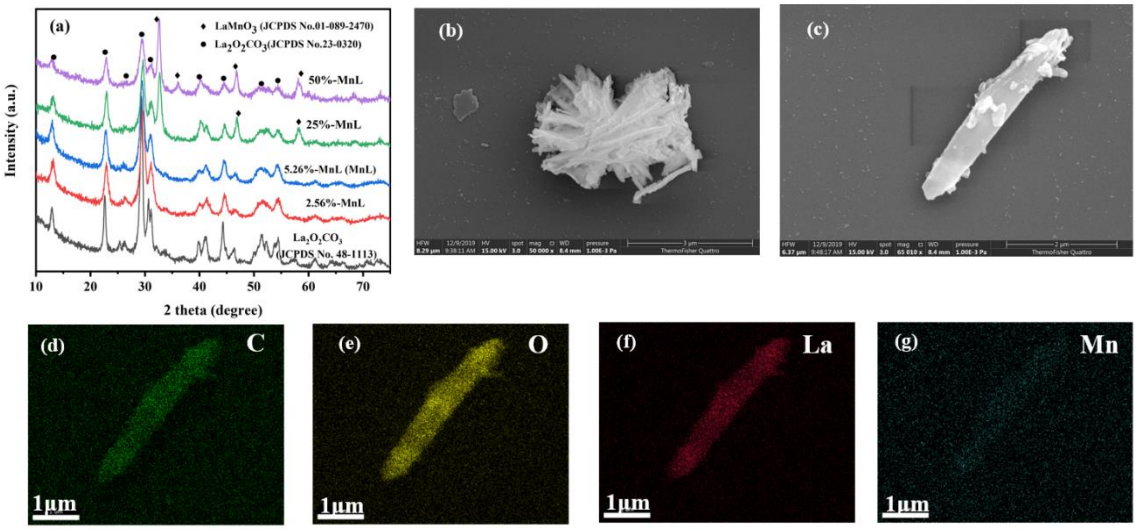

Fig. 1. (a) XRD patterns of Mn-doped $La_2O_2CO_3$ (MnL) with different amounts of Mn doping. (b-c) Representative ESEM images of MnL at different zoom levels, and element mapping images for (d) Carbon, (e) Oxygen, (f) Lanthanum and (g) Manganese, on MnL.

3.2. H_2O_2 activation by MnL for As(III) oxidation and further As(V) adsorption

3.2.1. The role of Mn content

The catalytic efficiency of the synthesised MnL for As(III) oxidation was firstly

evaluated under neutral conditions (Fig.2a). In the treatment group, containing H_2O_2 only without the addition of MnL, only 5% removal of As(III) was achieved, which indicated the low capability of As oxidation by H_2O_2 under such neutral conditions (Shan et al. 2019b). Additionally, the sole application of MnL could only remove approximately 3.5% of As(III) through adsorption, although it provided superior adsorption ability (555.6 mg L^{-1}) towards As(V). However, coupling H_2O_2/MnL achieved As(III) removal of up to 90% within 360 min (Fig. 2a), which indicated the great potential of MnL in catalysing H_2O_2 to oxidise As(III).

The dynamics of As(III) removal/oxidation could be well described (R^2>0.95) by the pseudo-first order model (Fig. S1a). Both removal efficiency of As(III) (Fig. 2a) and oxidation rate (k, Fig. S1a) improved to 90% and 0.0044 min^{-1}, respectively, with the increasing amount of Mn doping, from 0 (pure $La_2O_2CO_3$) to 5.26%, on $La_2O_2CO_3$. This might have occurred because the presence of variable-valence Mn atoms in the lattice structure of the materials could act as active sites, accelerating electron transfer during As(III) oxidation (Li et al. 2020, Tian et al. 2019, Zhou et al. 2020). However, both the As(III) removal efficiency and oxidation rate gradually reduced to 30% and 0.001 min^{-1}, respectively, under the higher Mn doping regime of 50% on $La_2O_2CO_3$. The excess Mn might have formed a new phase of $LaMnO_3$ in the lattice cell (Fig. 1), which may have caused a lack of exchangeable ligands, such as CO_3^{2-}, O^{2-} and -OH, between H_2O_2 and catalysts and might result in the decreased As(III) oxidation efficiency. This could be further supported by the observation that pure $LaMnO_3$ showed negligible catalytic effects on the oxidation of As(III) (Fig. S1b).

In order to completely remove As from contaminated water, further remediation of As(V), after prior oxidation of As(III), is necessary (Nicomel et al. 2016). The current result of the total As removal efficiencies (Fig. 2b) were identical to the As(III) oxidation/removal efficiencies (Fig. 2a) in the corresponding H_2O_2/MnL-coupled treatment system, indicating that the majority of the oxidation product of As(V) was adsorbed by MnL. This was supported by our previous study which determined that MnL can effectively adsorb As(V) through surface complexation, ion exchange and the formation of $LaAsO_4$ precipitates (Su et al. 2020). Overall, the results demonstrated that doping with Mn played a crucial role on H_2O_2 catalysis, and that the MnL material with Mn content of 5.26% performed the best at remediation of As through the synergistic functions of As(III) oxidation and As(V) adsorption.

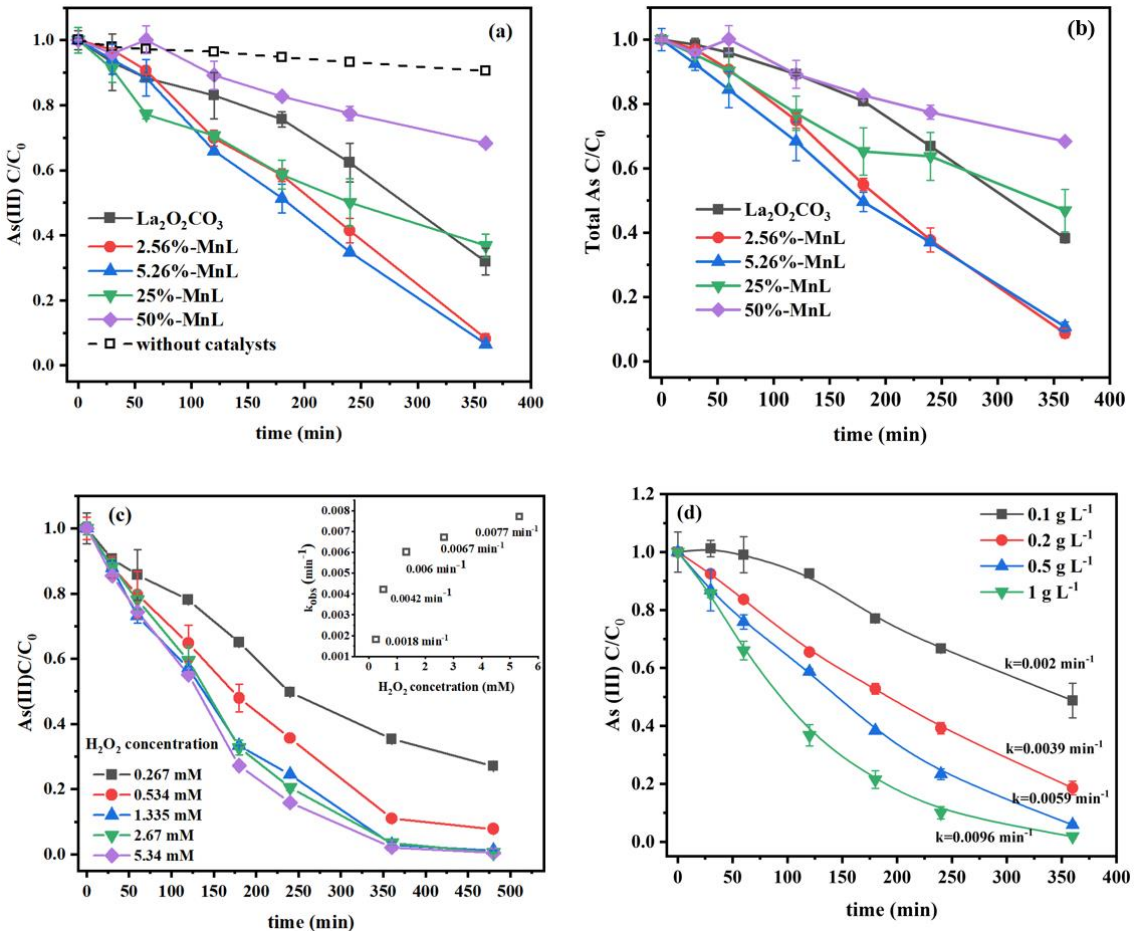

Fig. 2. (a) The kinetics of As(III) oxidation/removal and (b) total As removal from H_2O_2 oxidation systems with various Mn-doped $La_2O_2CO_3$ (MnL) catalysts under neutral conditions, and (c) the influences of initial H_2O_2 concentration and (d) MnL dosage, on As(III) removal.

3.2.2. The influences of H_2O_2 and MnL dosage

The best performance of As(III) oxidation was attributed to the MnL material doped with 5.26% Mn, which was therefore selected for further investigations to evaluate the influencing factors during the reactions. In the treatment system using H_2O_2/MnL coupling, the oxidation rate of As(III) was found to increase dramatically when H_2O_2 concentration increased from 0.267 mM (oxidation rate: 0.0018 min^{-1}) to 1.335 mM (0.006 min^{-1}) (Fig. 2c). Correspondingly, the oxidation efficiency of As(III) increased from 73% to 99% within 480 min. However, with further increasing H_2O_2 dosage to 5.34 mM, the As(III) oxidation rate only exhibited slight improvement, to 0.0077 min^{-1}. This might have been due to the gradual saturation of sites for H_2O_2 adsorbed on the MnL, thus limiting As(III) oxidation (Gennari et al. 2015). Additionally, increasing the dosage of MnL was observed to improve As(III) oxidation (Fig. 2d). Oxidation efficiency increased from 51% to 98% within 360 min when the addition of MnL increased from 0.1 to 1 g L^{-1}, which could be ascribed to the availability of more active surficial catalytic sites at higher dosages of MnL (Kim et al. 2015). Therefore, the optimum ratio of the H_2O_2 and MnL should be carefully determined for As(III) oxidation, in order to achieve the best

performance.

3.2.3. The influence of pH

It has been reported that pH is an important factor influencing As(III) oxidation by H_2O_2. The current determination that H_2O_2-only treatment of As(III) at pH 11 reached similar removal efficiency (~90% within 30 min) to that under MnL catalysis treatment (Fig. 3a), agreed with previous work that showed direct oxidation by H_2O_2 only occurred under strong alkaline conditions (Qian et al. 2015, Shan et al. 2019b). Significantly lower As(III) oxidation efficiencies (<22%) were obtained under acid or neutral conditions (pH of 3-7).

By contrast, in the H_2O_2/MnL -coupled treatment system, similar oxidation efficiencies of As(III) were achieved (88%) under neutral conditions (pH 7) when compared with the reaction under strong alkaline conditions (pH of 11). At pHs of 5 and 9, the oxidation efficiencies were approximately 70% within 360 min. In strong acid conditions (pH 3), the oxidation efficiency (18.5%) of As(III) was much lower when compared with those values obtained under other pH conditions. This might be due to the poor stability of MnL under strong acid, where the amount of La and Mn leaching at pH 3 was as high as 283 and 3.5 mg L^{-1}, respectively (Fig. 3b). These amounts were almost equal to the original contents of La and Mn in the studied MnL composites.

The production of As(V) has also been detected in the H_2O_2/MnL-coupled treatment system (Fig. 3c). In the pH 5-9 range, the concentrations of As(V) in solution increased within the initial 30 min and then decreased gradually thereafter, indicating that the removal process of As(III) by MnL was through the combination of As(III) oxidation and As(V) adsorption. However, As(V) in solution displayed a negligible decrease after 30 min at both pH=3 and 11, which may have been due to i) active surfaces on MnL being dissociated in the strong acid conditions and ii) MnL possessing poor adsorption qualities towards As(V) under strong alkaline conditions (Xu et al. 2018). The total As removal performance of the proposed heterogenous catalytically treatment system (Fig. 3d), indicated that the MnL/H_2O_2 -coupled catalytic system could achieve both efficient As(III) oxidation and As(V) removal over the wide pH range of 5-9.

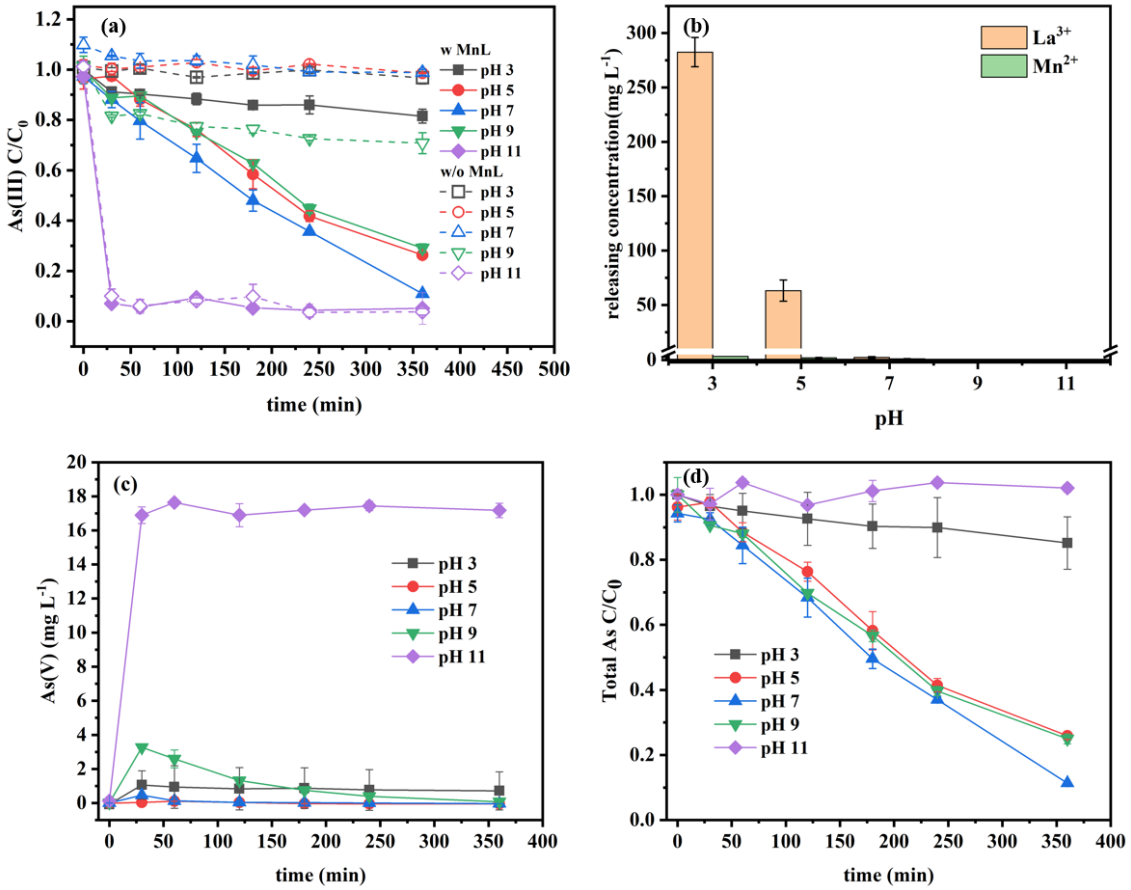

Fig. 3. (a) As(III) oxidation in the MnL/H_2O_2 and H_2O_2-only treatment systems under various pH conditions. (b) Amounts of La and Mn released under various pH conditions in the MnL/H_2O_2 -coupled system. (c) As(V) generation and (d) total As removal, in the MnL/H_2O_2 -coupled treatment system, under various pH conditions.

3.3. Mechanisms of As(III) oxidation in the MnL/H_2O_2 -coupled system

3.3.1. The functions of reactive species

Reactive oxygen species (ROSs), i.e. hydroxyl (·OH), hydroperoxyl (·OOH) and superoxide radicals ($\cdot O_2^-$), are recognized as important oxidants in catalysed H_2O_2 oxidation reactions (Watts and Teel 2019). In this study, ESR spectroscopy detected the typical peaks of the DMPO-OOH adduct with an intensity ratio of 1:1:1:1 from samples collected from MnL/H_2O_2 -coupled treatment systems (Fig. 4a), supporting the formation over MnL of $\cdot O_2^-$/·OOH. Moreover, the presence of the DMPO-OH adduct (intensity ratio of 1:2:2:1) was additionally observed within 2 min (Fig. 4b), which suggested the formation of ·OH, and this might be ascribed to a Fenton-like reaction, activated by ≡Mn(II/III) (Weng et al. 2017). However, after 2 min, the signal for DMPO-OH disappeared, which might have indicated that ·OH was quickly consumed by the excess of H_2O_2, or by the pristine CO_3^{2-} in the material following the reactions in Eq. 6-8 (Jiang et al. 2020, Zhou et al. 2020):

$$H_2O_2 + \cdot OH \rightarrow H_2O + \cdot O_2H \quad (k=2.7\times10^7\ M^{-1}S^{-1}) \tag{6}$$

$$\cdot OH + CO_3^{2-} \rightarrow \cdot CO_3^- + OH^- \tag{7}$$

$$\cdot OH + HCO_3^- \rightarrow \cdot HCO_3 + OH^- \ldots CO_2 + OH^- \tag{8}$$

In order to evaluate the specific role of each radical, scavenging compounds, *viz*. tert-butyl alcohol (TBA) and p-benzoquinone (p-BQ) (Kim et al. 2015), were added to the MnL/H_2O_2 system during the reaction (Fig. 4c). Following the addition of TBA (100 mM), the ·OH scavenger ($k_{\cdot OH/TBA}$= 3.0×10^9 M^{-1} S^{-1}), the As(III) oxidation efficiency did not show significant change when compared with the control group, which indicated that the ·OH may not have been the main radical responsible for As(III) oxidation. By contrast, the oxidation efficiency of As(III) decreased from 90% to 53% within 360 min with addition of 1 mM p-BQ ($k_{\cdot O2^-/BQ}$=1.0×10^9 M^{-1} S^{-1}), and this further decreased to 18% when the concentration of p-BQ was increased to 5 mM. The results suggested that $\cdot O_2^-$ /·OOH rather than ·OH played the major role in As(III) oxidation in the MnL/H_2O_2 treatment system.

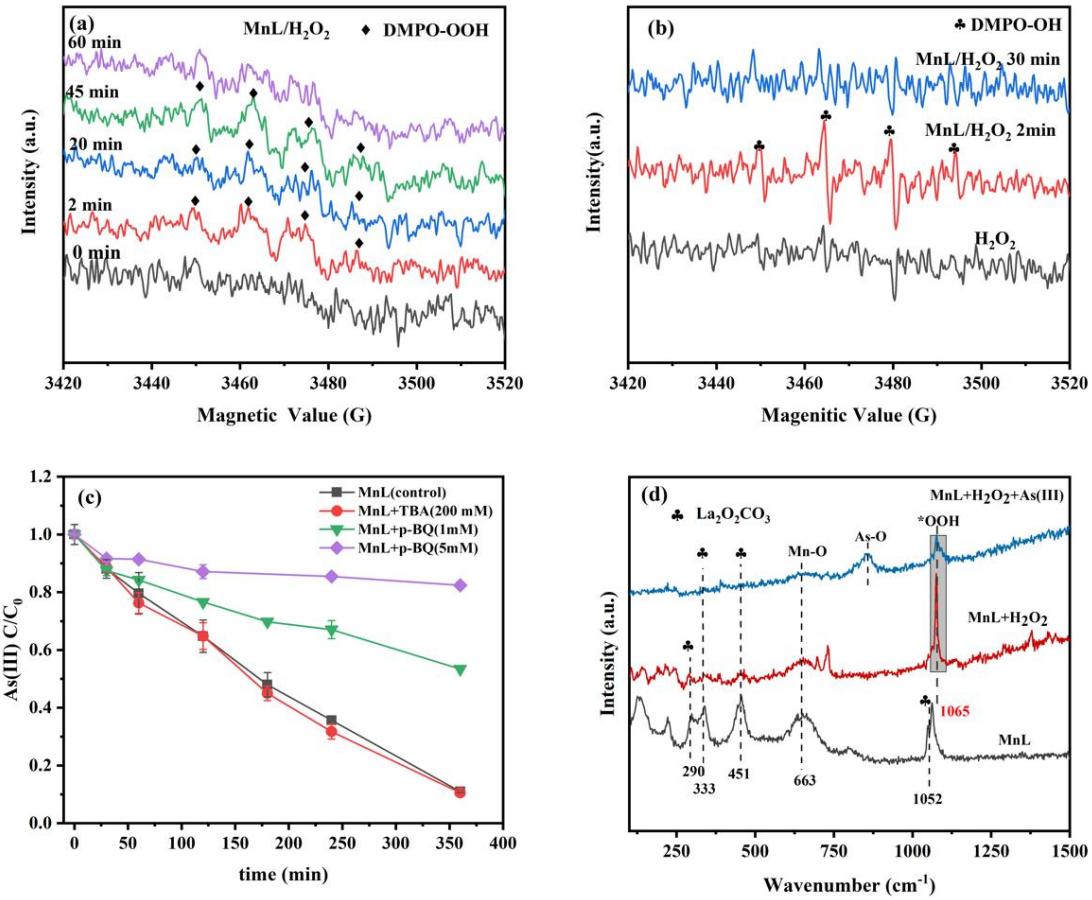

Fig. 4. (a) ESR spectra of DMPO-OOH and (b) DMPO-OH formed in the MnL/H_2O_2 -coupled system. (c) Effect of quenching agents on As(III) oxidation by MnL/H_2O_2 -coupled treatment. (d) Raman spectra of MnL in the presence or absence of H_2O_2 and in the presence of As(III).

3.3.2. The origin of $\cdot O_2^-$/·OOH

In addition to H_2O_2, dissolved oxygen may be an important source for O_2^-/·OOH

formation in some catalysis reactions (Exner and Over, 2019). To investigate this, the MnL/H_2O_2 coupling treatments were conducted separately, in solutions that were aerated either by O_2 or N_2 (Fig. S2a). It was clear that the excess oxygen did not show a significant positive effect on As(III) oxidation. Meanwhile, there was only a slight suppression of efficiency of As(III) oxidation under N_2 conditions. These observations thus excluded the role of dissolved oxygen for $\cdot O_2^-$ production and contribution to As(III) oxidation.

It was known that La(III) could catalyse, as a Lewis acid-base adduct, the epoxidation of olefins, by forming a peroxide complex with H_2O_2, resulting in the generation of ROSs (Novikov et al. 2016). After treatment, the DR-UVS spectrum of MnL showed an obvious red shift (Fig. S2b), and a new characteristic band (1065 cm^{-1}) was observed in the Raman spectrum (Fig. 4d) that could be assigned to peroxide species (Shan et al. 2019b, Wang et al. 2018, Wei et al. 2019). The results suggested that H_2O_2 was substantially adsorbed onto MnL and formed a surficial Lewis acid-base adduct, i.e. La-OOH*, through the reaction in Eq. 9 (Corma and Garcı´a 2002). This Lewis acid-base complex would be then dissociated by donating electrons towards La(III) sites (Eq. 10), giving rise to the formation of surficial $\cdot O_2^-$/·OOH species (Novikov et al. 2016), finally causing conversion of As(III) to As(V) (Eq. 11).

$$\equiv La - OH + H_2O_2 \rightarrow \equiv La - OOH* + H_2O \quad (9)$$

$$\equiv La - OOH* \rightarrow \equiv La -\cdot OOH \quad (10)$$

$$\equiv La -\cdot OOH + As^{III}(OH)_3 \rightarrow \equiv La - OH + OAs^{V}(OH)_3 \quad (11)$$

Further experimentation with addition of NaF, acting as inhibitor towards La(III) (Wu et al. 2018), greatly reduced As(III) oxidation (Fig. S2c), confirming the important role of ≡La(III) sites on H_2O_2 decomposition. It is hypothesised that, due to the effective complexation ability and the electrophilic properties of La(III), the surficial radical La-·OOH was able to be stabilized and extend the lifetime of ·OOH to at least 60 minutes (Fig. 4a). During As(III) oxidation, the intensity of the peak attributed to La-OOH* in acquired Raman spectra (Fig. 4d) dramatically decreased, accompanied by an appearance of a signal due to the As-O species. It could thus be concluded that the surficial Lewis acid-base complex (La-OOH*) was an important precursor of $\cdot O_2^-$/·OOH generation.

3.3.3. The effects of different-valent Mn

As an active transition metal with various valence states, Mn has been demonstrated to typically show a positive effect on both pollutant adsorption and catalytic oxidation reactions (Wen et al. 2017, Weng et al. 2017). During the H_2O_2 catalytic oxidation by MnL, the content of Mn(IV) in MnL increased from 36.5% to 44.8% while Mn(III) and Mn(II) decreased from 34.2% to 26.5% and 29.3% to 28.5%,

respectively (Fig. 5a). However, during the As(III) adsorption reaction by MnL alone, without the addition of H_2O_2, the contents of Mn(II), Mn(III) and Mn(IV) in MnL exhibited negligible change.

Since Mn can act as a typical active site for Fenton-like reactions, Mn with low valence states, i.e. Mn(II), Mn(III), could be oxidised by H_2O_2 accompanied by Mn(IV) and ·OH production (Eq. 12-13). Meanwhile, Mn(III), acting as Lewis acid might also complex and dissociate H_2O_2 to produce ·OOH (Eq. 14). Therefore, the decrease in content of Mn(III) in MnL would be significantly higher than that of Mn(II), when MnL was treated with H_2O_2. After oxidizing As(III), a small amount of Mn(IV) would have been reduced to Mn(II) and Mn(III) again (Eq. 15), which might be attributed to As(III) being directly oxidised by Mn(IV)-OH under the acidic conditions (Zhang et al. 2018). However, compared to ·OOH, the role of Mn(IV) for As(III) oxidation would be considered to be minor.

$$\equiv Mn(II) + H_2O_2 \rightarrow \equiv Mn(III) + OH^- + \cdot OH \quad (12)$$

$$\equiv Mn(III) + H_2O_2 \rightarrow \equiv Mn(IV) + OH^- + \cdot OH \quad (13)$$

$$\equiv \mathrm{Mn(III)} + \mathrm{H_2O_2} + 2\mathrm{OH^-} \rightarrow \equiv \mathrm{Mn(II)} + \cdot \mathrm{O_2^-} + 2\mathrm{H_2O} \quad (14)$$

$$\equiv Mn(IV) - OH + As(III) + H^+ \rightarrow \equiv Mn(II/III) - OH + As(V) \quad (15)$$

It should be noted that newly formed ·OH through a Fenton-like reaction would be quenched rapidly by CO_3^{2-}/HCO_3^- (Eq. 7-8), thus the utilisation efficiency of H_2O_2 for A_S(III) oxidation in MnL activating system (52.5%-64.3%) was obviously lower than that in pure $La_2O_2CO_3$ system (77.4%-91.5%) (Fig. S2d). Nevertheless, the adsorption efficiency of H_2O_2 on MnL was greatly improved, as shown in Fig. 5b-c, which would facilitate the formation of surficial Lewis acid-base complexes and favour ROS production. In addition, because of the valence state transformation between Mn(II)/Mn(III) and Mn(IV) during oxidation of As(III), interfacial electron transfer would have been accelerated and that gave rise to higher current density during the reaction (Fig. 5d), which efficiently promoted oxidation of As(III) (Tian et al. 2019).

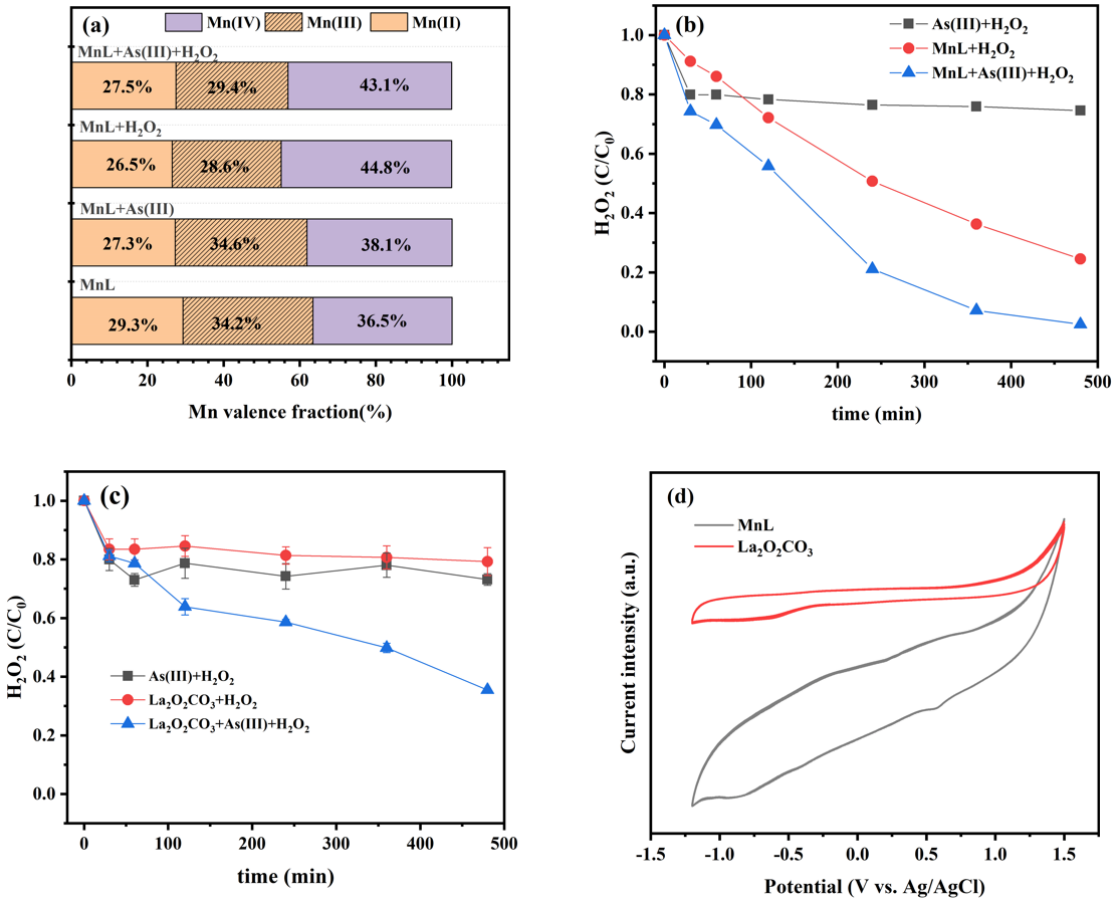

Fig. 5. (a) Fractions of Mn species under different treatment conditions, (b) evolution of H_2O_2 by MnL activation with and without As(III) addition, (c) evolution of H_2O_2 by pure $La_2O_2CO_3$ activation with and without As(III) addition and (d) cyclic voltammetry plots of MnL and pure $La_2O_2CO_3$ in 0.267 mM H_2O_2 and 50 mg L^{-1} As(III).

3.3.3. The overall processes of As removal

XRD spectra of MnL clearly showed the formation of $LaAsO_4$ precipitates (JCPDS card. No. 15-0756) after As(III) oxidation (Fig. 6a), consistent with the ESEM image that revealed wire-like species present on the MnL rod (Fig. S3), suggesting that La(III) sites also played an important role on As(V) immobilisation. The absence of manganese arsenic compounds in XRD spectra might be ascribed to the minor amount of Mn present in MnL, thus the corresponding peaks of products were not evident. XPS spectra of As3d (Fig. 6b) elucidated that all of the immobilized arsenic on MnL, including the pre-adsorbed As(III) (44.5 eV), had been completely converted to As(V) (45.3 eV) (Ma et al. 2020) in the MnL/H_2O_2 -coupled system. XPS spectra of C1s (Fig. 6c) supported that CO_3^{2-} (289.4 eV) (Liu et al. 2018) in MnL decreased from 22.6% to 19.1% after As(III) removal, indicating that the adsorption process of As(V) on MnL was accompanied by CO_3^{2-}/HCO_3^- exchange (Su et al. 2020). For O1s, La/Mn-O peak (528.8 eV) decreased markedly, while the As-O signal (531.0 eV) was present after As(III) oxidation(Fig. 6d), well supporting the fact that La/Mn were active sites for As(V) adsorption (Lv et al. 2019). It should be noted that the percentage ratio of surface oxygen, i.e. -OH/OOH (531.4 eV) in MnL increased

from 59.5% to 60.9% after H_2O_2 treatment, confirming the formation of the lanthanum/peroxide complex, La-OOH*. However, the intensity of surface -OH/-OOH had decreased again to 49.6%, proving that the surface peroxide complex was consumed by arsenite during oxidation, which was in accordance with the result of Raman analysis (Fig. 4d).

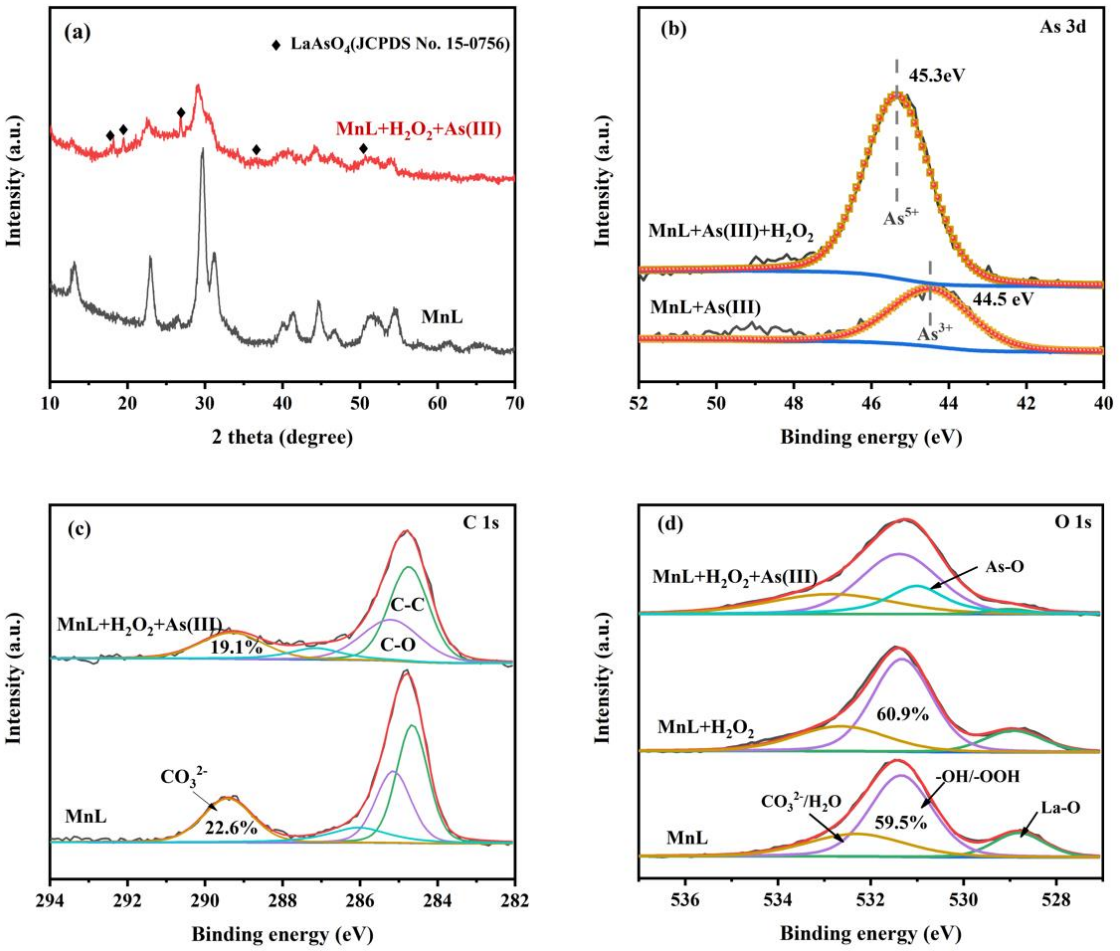

Fig. 6. (a) XRD spectra of MnL, (b) XPS spectra of As3d, (c) C1s and (d) O1s of MnL, before and after As(III) oxidation.

In summary, the removal process of As in the MnL/H_2O_2 coupling system can be visualised in Fig.7. Initially, part of the As(III) could be directly oxidised by H_2O_2, however the amount would be relatively low under neutral and acid conditions (Shan et al. 2019b). The majority of the As(III) would be oxidised to As(V) by the generated ROSs. La(III) sites would have played an important role in complexing with H_2O_2 to form surficial Lewis acid-base complex species, which were the precursors of ·OOH and produced the dominant effect on As(III) oxidation. Mn(III) ions in MnL also acted as activators to improve ·OOH production by adsorbing and dissociating H_2O_2. Meanwhile, Mn in low valence states (Mn(II/III)) might accelerate charge transfer processes during As(III) oxidation by a Fenton-like reaction, which finally induced highly efficient decontamination of As(III). The As(V) oxidised from As (III) and original As(V) would be

rapidly adsorbed on La and Mn lattice sites in MnL by precipitation, accompanied with exchange with CO_3^{2-}/HCO_3^-. Thus, this H_2O_2 catalysis system would finally achieve effective removal of As in contaminated water.

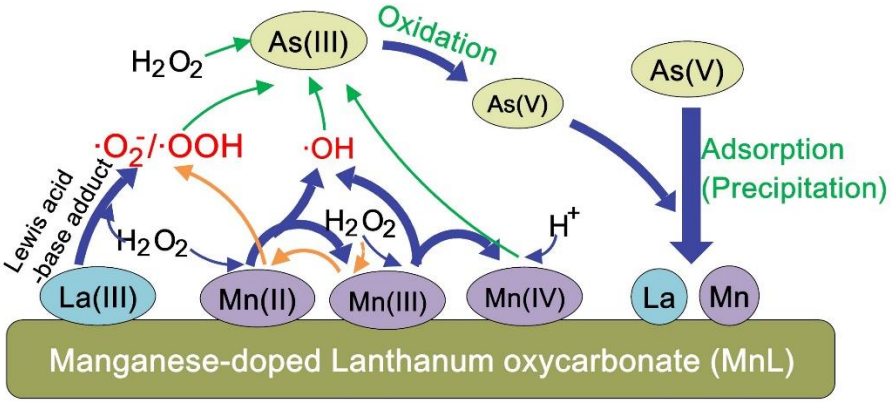

Fig.7 The removal processes of As in MnL/H_2O_2 -coupled system

3.4. The effect of coexisting ions on As(III) removal and reusability of MnL

The oxidation efficiency of As(III) increased from 92% to 98% when 0.2 mM Fe^{3+} was present in the MnL/H_2O_2 -coupled reaction solution, indicating that an appropriate amount of Fe^{3+} was conducive to As(III) oxidation (Fig. 8a). It is known that Fe^{3+}, as an active transition metal, can catalyse H_2O_2 to generate ·OOH and Fe^{2+} and accelerate electron transfer and facilitate ROS production (Zhou et al. 2020), and thus might cause the improvement of As(III) oxidation. Meanwhile, Fe^{3+} could rapidly capture the oxidation product, $HAsO_4^{2-}$ by forming precipitates of $FeAsO_4$ (Zhang et al. 2019), further contributing to the highly-efficient removal of As(III). However, when increasing the concentration of Fe^{3+} to 2 mM, the removal efficiency of As (III) sharply decreased to 10%, probably because the strongly acidic conditions (pH 2.98) under a high concentration of Fe^{3+} would destabilize the catalyst and lead to a significant loss of active sites (Fig. 3b).

When Mn^{2+} or Cl^- were present in the solution, the removal efficiency of As(III) was maintained between 92% to 94%, indicating that these ions had little impact on As(III) removal. Although Mn^{2+} was able to catalyse H_2O_2 to produce ·OH (Eq. 12), the newly formed ·OH would be rapidly quenched by CO_3^{2-} in MnL so that the presence of free Mn^{2+} could not significantly promote the oxidation and removal of As(III). It could also be seen that the presence of $H_2PO_4^-$ and HCO_3^- had little influence on As(III) oxidation at low concentration (0.2 mM) while showing substantial inhibitory effect at the higher concentration studied (2 mM). This might be attributed to the excess amount of phosphoric acid and carbonic acid competing with As(III) for La lattice sites, thus hindering the adsorption of As(V) (Su et al. 2020), reducing the catalytic activity of MnL and decreasing the removal efficiency of As(III). Additionally, HCO_3^-, as a quencher of most ROSs (Eq. 7-8), further reduced the oxidation efficiency of As(III) to 65% when the

concentration reached 2 mM.

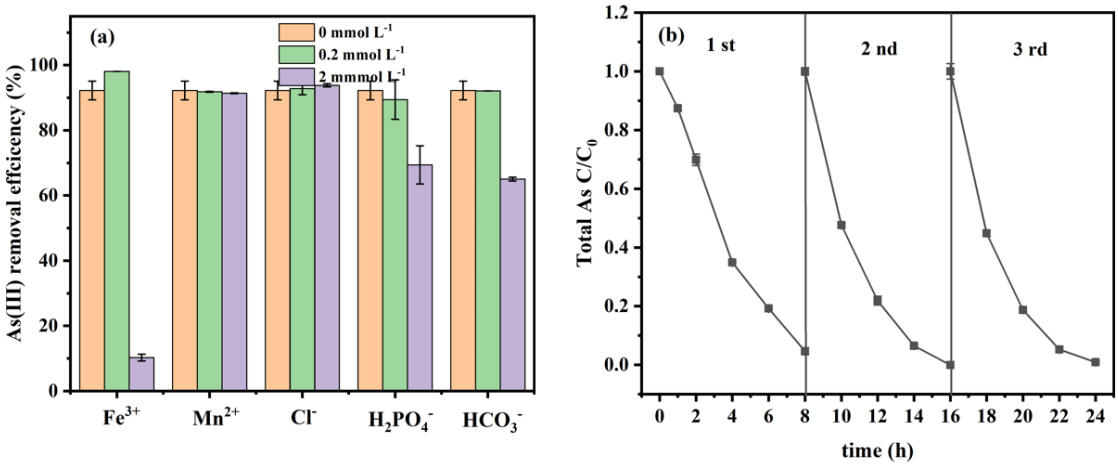

Fig. 8 (a) The effect of coexisting ions on As(III) removal in MnL/H_2O_2 system**.** (b) The removal efficiency of As(III) over sequential MnL regeneration cycles.

In addition, the reusability of MnL as a catalyst of H_2O_2 oxidation, for the removal of As, was evaluated (Fig. 8b). After three cycles of As(V) desorption followed by MnL regeneration with NaOH (1 M), the catalyst could still achieve 99% removal of As within 8 h (Fig. 8b), which suggested that MnL, as a catalyst and adsorbent, possessed good stability and reusability. Notably, the removal rate of As in the second and third cycles was slightly higher than that in the first, which has been interpreted as a consequence of decreases in the content of CO_3^{2-} in MnL after successive regeneration treatments with NaOH. Since CO_3^{2-} showed an adverse effect on ROS production and As(V) adsorption, the presence of less CO_3^{2-} would conceivably increase As(III) removal. Additionally, remnant As(III) in solution was less than 9.8 and 6.0 μg L^{-1} from an initial As(III) concentration of 3.15 mg L^{-1}, when treated by MnL dosages of 0.2 and 0.5 g L^{-1}, respectively (Fig. S5). These final As values were below the permissible value stated in the drinking water standard regulated by WHO (Wei et al. 2019), further suggesting that MnL presents an encouraging prospect for As removal, through the catalysis of H_2O_2 oxidation.

4. Conclusions

In this study, Mn-doped $La_2O_2CO_3$ (MnL) was proved to be a good catalyst for oxidation of As(III) by H_2O_2, over a wide pH range of 5-9, which greatly broadens the applicability of this oxidant. Mechanistic studies revealed that La lattice sites played an important role in generating surficial superoxide radicals ($\cdot O_2^-$/·OOH) by forming an active Lewis acid-base adduct (La-OOH*) with H_2O_2, and persistent surficial $\cdot O_2^-$/·OOH was confirmed to be the dominant active species available for As(III) oxidation. Meanwhile, the low-valent states of Mn (Mn(II/III)) not only accelerated charge transfer during the oxidation, but also improved ·OOH production and the adsorption of H_2O_2 on the surface of MnL,

which resulted in higher oxidation efficiency of As(III). The oxidation product As(V) would then be rapidly immobilized on the La and Mn sites by forming precipitates. This work thus provides a new strategy by which to develop other Lanthanum-based catalysts for environmental remediation by advanced oxidation processes. Moreover, the excellent reusability of the MnL material and the levels of remnant As well below the permissive value (10 μg L^{-1}) after treatment, further suggested that remediation by the MnL/H_2O_2-couple is a great prospect for the effective and simultaneous oxidation of As(III) and adsorption of As(V) towards complete As elimination.

Acknowledgements

This work was supported by the National Key R&D Program of China (2017YFA0207204), and the National Natural Science Foundation of China (Grant No. 21806175). We also acknowledge the financial support of Hunan Zhongke Water Environmental Management Co., Ltd., and Yantai HABs Control and Ecological Restoration Technology Co. Ltd., through their cooperation projects with Nottingham Trent University.

Reference

Ahmad, S.A., Khan, M.H. and Haque, M. (2018) Arsenic contamination in groundwater in Bangladesh: implications and challenges for healthcare policy. Risk Management and Healthcare Policy 11, 251.

Argos, M., Ahsan, H. and Graziano, J.H. (2012) Arsenic and human health: epidemiologic progress and public health implications. Reviews on environmental health 27(4), 191-195.

Chen, F., Shen, X., Wang, Y. and Zhang, J. (2012) CeO_2/H_2O_2 system catalytic oxidation mechanism study via a kinetics investigation to the degradation of acid orange 7. Applied Catalysis B: Environmental 121-122, 223-229.

Corma, A. and Garcı´a, H. (2002) Lewis Acids as Catalysts in Oxidation Reactions From Homogeneous to Heterogeneous Systems. Chemical Reviews 102, 3837-3892.

Ding, W., Xu, J., Chen, T., Liu, C., Li, J. and Wu, F. (2018) Co-oxidation of As(III) and Fe(II) by oxygen through complexation between As(III) and Fe(II)/Fe(III) species. Water Res 143, 599-607.

Exner, K.S. and Over, H. (2019) Beyond the rate-determining step in the oxygen evolution reaction over a single-crystalline IrO2 (110) model electrode: kinetic scaling relations. Acs Catalysis 9(8), 6755-6765.

Fernandes, C.I., Vaz, P.D., Nunes, T.G. and Nunes, C.D. (2020) Zinc biomimetic catalysts for epoxidation of olefins with H_2O_2. Applied Clay Science 190.

Gennari, M., Brazzolotto, D., Pécaut, J., Cherrier, M.V., Pollock, C.J., DeBeer, S., Retegan, M., Pantazis, D.A., Neese, F. and Rouzières, M. (2015) Dioxygen activation and catalytic reduction to hydrogen peroxide by a thiolate-bridged dimanganese (II) complex with a pendant thiol. Journal of the American Chemical Society 137(26), 8644-8653.

Jiang, W., Dionysiou, D.D., Kong, M., Liu, Z., Sui, Q. and Lyu, S. (2020) Utilization of formic acid in nanoscale zero valent iron-catalyzed Fenton system for carbon tetrachloride degradation. Chemical Engineering Journal 380.

Kim, D.H., Bokare, A.D., Koo, M. and Choi, W. (2015) Heterogeneous catalytic oxidation of As(III) on nonferrous metal oxides in the presence of H_2O_2. Environ Sci Technol 49(6), 3506-3513.

Li, H., Gao, Q., Wang, G., Han, B., Xia, K. and Zhou, C. (2020) Unique electron reservoir properties of manganese in Mn(II)-doped CeO_2 for reversible electron transfer and enhanced Fenton-like catalytic performance. Applied Surface Science 502.

Liu, X., Zong, E., Hu, W., Song, P., Wang, J., Liu, Q., Ma, Z. and Fu, S. (2018) Lignin-Derived Porous Carbon Loaded with $La(OH)_3$ Nanorods for Highly Efficient Removal of Phosphate. ACS Sustainable Chemistry & Engineering 7(1), 758-768.

Lv, Z., Fan, Q., Xie, Y., Chen, Z., Alsaedi, A., Hayat, T., Wang, X. and Chen, C. (2019) MOFs-derived magnetic chestnut shell-like hollow sphere NiO/Ni@C composites and their removal performance for arsenic(V). Chemical Engineering Journal 362, 413-421.

Ma, L., Cai, D. and Tu, S. (2020) Arsenite simultaneous sorption and oxidation by natural ferruginous manganese ores with various ratios of Mn/Fe. Chemical Engineering Journal 382.

Manning, B.A., Fendorf, S.E., Bostick, B. and Suarez, D.L. (2002) Arsenic (III) oxidation and arsenic (V) adsorption reactions on synthetic birnessite. Environmental science & technology 36(5), 976-981.

Muthu Prabhu, S., Chuaicham, C. and Sasaki, K. (2018) A Mechanistic Approach for the Synthesis of Carboxylate-Rich Carbonaceous Biomass-Doped Lanthanum-Oxalate Nanocomplex for Arsenate Adsorption. ACS Sustainable Chemistry & Engineering 6(5), 6052-6063.

Nicomel, N.R., Leus, K., Folens, K., Van Der Voort, P. and Du Laing, G. (2016) Technologies for arsenic removal from water: current status and future perspectives. International journal of environmental research and public health 13(1), 62.

Novikov, A.S., Kuznetsov, M.L., Rocha, B.G.M., Pombeiro, A.J.L. and Shul'pin, G.B. (2016) Oxidation of olefins with H_2O_2 catalysed by salts of group III metals (Ga, In, Sc, Y and La): epoxidation versus hydroperoxidation. Catalysis Science & Technology 6(5), 1343-1356.

Qian, A., Yuan, S., Zhang, P. and Tong, M. (2015) A New Mechanism in Electrochemical Process for Arsenic Oxidation: Production of H_2O_2 from Anodic O_2 Reduction on the Cathode under Automatically Developed Alkaline Conditions. Environ Sci Technol 49(9), 5689-5696.

Qiu, Z., Shi, S., Qiu, F., Xu, X., Yang, D. and Zhang, T. (2020) Enhanced As(Ш) removal from aqueous solutions by recyclable Cu@MNM composite membranes via synergistic oxidation and absorption. Water Research 168.

Shan, C., Dong, H., Huang, P., Hua, M., Liu, Y., Gao, G., Zhang, W., Lv, L. and Pan, P. (2019a) Dual-functional millisphere of anion-exchanger-supported nanoceria for synergistic As(III) removal with stoichiometric H_2O_2 Catalytic oxidation and sorption. Chemical Engineering Journal 360, 982-989.

Shan, C., Liu, Y., Huang, Y. and Pan, B. (2019b) Non-radical pathway dominated catalytic oxidation of As(III) with stoichiometric H_2O_2 over nanoceria. Environ Int 124, 393-399.

Smith, A.H., Marshall, G., Liaw, J., Yuan, Y., Ferreccio, C. and Steinmaus, C. (2012) Mortality in young adults following in utero and childhood exposure to arsenic in drinking water. Environmental health perspectives 120(11), 1527-1531.

Su, J., Lyu, T., Yi, H., Bi, L. and Pan, G. (2020) Superior arsenate adsorption and comprehensive investigation of adsorption mechanism on novel Mn-doped $La_2O_2CO_3$ composites. Chemical Engineering Journal, 123623.

Su, X., Kushima, A., Halliday, C., Zhou, J., Li, J. and Hatton, T.A. (2018) Electrochemically-mediated

selective capture of heavy metal chromium and arsenic oxyanions from water. Nature communications 9(1), 1-9.

Tian, N., Tian, X., Nie, Y., Yang, C., Zhou, Z. and Li, Y. (2019) Enhanced 2, 4-dichlorophenol degradation at pH 3–11 by peroxymonosulfate via controlling the reactive oxygen species over Ce substituted 3D Mn_2O_3. Chemical Engineering Journal 355, 448-456.

Wahlen, J., De Vos, D., De Hertogh, S., Nardello, V., Aubry, J.M., Alsters, P. and Jacobs, P. (2005) Lanthanum-exchanged zeolites as active and selective catalysts for the generation of singlet oxygen from hydrogen peroxide. Chem Commun (Camb) (7), 927-929.

Wang, C., Yin, H., Bi, L., Su, J., Zhang, M., Lyu, T., Cooper, M. and Pan, G. (2020) Highly efficient and irreversible removal of cadmium through the formation of a solid solution. Journal of hazardous materials 384, 121461.

Wang, T., Yang, W., Song, T., Li, C., Zhang, L., Wang, H. and Chai, L. (2015) Cu doped Fe_3O_4 magnetic adsorbent for arsenic: synthesis, property, and sorption application. RSC Advances 5(62), 50011-50018.

Wang, W., Zhu, Q., Qin, F., Dai, Q. and Wang, X. (2018) Fe doped CeO_2 nanosheets as Fenton-like heterogeneous catalysts for degradation of salicylic acid. Chemical Engineering Journal 333, 226-239.

Watts, R.J. and Teel, A.L. (2019) Hydroxyl radical and non-hydroxyl radical pathways for trichloroethylene and perchloroethylene degradation in catalyzed H2O2 propagation systems. Water research 159, 46-54.

Wei, Y., Yu, X., Liu, C., Ma, J., Wei, S., Chen, T., Yin, K., Liu, H. and Luo, S. (2019) Enhanced arsenite removal from water by radially porous Fe-chitosan beads: Adsorption and H_2O_2 catalytic oxidation. J Hazard Mater 373, 97-105.

Wen, Z., Zhang, Y., Wang, Y., Li, L. and Chen, R. (2017) Redox transformation of arsenic by magnetic thin-film MnO_2 nanosheet-coated flowerlike Fe_3O_4 nanocomposites. Chemical Engineering Journal 312, 39-49.

Weng, Z., Li, J., Weng, Y., Feng, M., Zhuang, Z. and Yu, Y. (2017) Surfactant-free porous nano-Mn_3O_4 as a recyclable Fenton-like reagent that can rapidly scavenge phenolics without H_2O_2. Journal of Materials Chemistry A 5(30), 15650-15660.

Wu, P., Xia, L., Liu, Y., Wu, J., Chen, Q. and Song, S. (2018) Simultaneous Sorption of Arsenate and Fluoride on Calcined Mg–Fe–La Hydrotalcite-Like Compound from Water. ACS Sustainable Chemistry & Engineering 6(12), 16287-16297.

Xu, H., Wang, D., Ma, J., Zhang, T., Lu, X. and Chen, Z. (2018) A superior active and stable spinel sulfide for catalytic peroxymonosulfate oxidation of bisphenol S. Applied Catalysis B: Environmental 238, 557-567.

Xu, R., Lyu, T., Zhang, M., Cooper, M. and Pan, G. (2020) Molecular-level investigations of effective biogenic phosphorus adsorption by a lanthanum/aluminum-hydroxide composite. Science of The Total Environment 725, 138424.

Xuan, K., Zhu, X., Cai, Y. and Tu, X. (2018) Plasma oxidation of H2S over non-stoichiometric LaxMnO3 perovskite catalysts in a dielectric barrier discharge reactor. Catalysts 8(8), 317.

Yang, X., He, J., Yang, Q., Jiao, R., Liao, G. and Wang, D. (2019) Cu(I)-doped Fe_3O_4 nanoparticles/porous C composite for enhanced H_2O_2 oxidation of carbamazepine. J Colloid Interface Sci 551, 16-25.

Zhang, W., Liu, C., Zheng, T., Ma, J., Zhang, G., Ren, G., Wang, L. and Liu, Y. (2018) Efficient

oxidation and sorption of arsenite using a novel titanium(IV)-manganese(IV) binary oxide sorbent. J Hazard Mater 353, 410-420.

Zhang, W., Liu, F., Sun, Y., Zhang, J. and Hao, Z. (2019) Simultaneous redox conversion and sequestration of chromate(VI) and arsenite(III) by iron(III)-alginate based photocatalysis. Applied Catalysis B: Environmental 259.

Zhou, X., Xu, D., Chen, Y. and Hu, Y. (2020) Enhanced degradation of triclosan in heterogeneous E-Fenton process with MOF-derived hierarchical Mn/Fe@PC modified cathode. Chemical Engineering Journal 384.

Supporting Information

Efficient Arsenic (As) removal by manganese-doped Lanthanum oxycarbonate enabled with enhanced H_2O_2 catalytic oxidation of As(III) and adsorption of As(V)

Jing Su[a,b], Tao Lyu*[c], Mick Cooper[d], Gang Pan*[a,b,d]

[a] *Key Laboratory of Environmental Nanotechnology and Health Effects, Research Center for Eco-Environmental Sciences, Chinese Academy of Sciences, Beijing 100085, P. R. China*

[b] *University of Chinese Academy of Sciences, Beijing 100049, P. R. China*

[c] *Cranfield Water Science Institute, Cranfield University, College Road, Cranfield, Bedfordshire, MK43 0AL, UK*

[d] *School of Animal, Rural, and Environmental Sciences, Nottingham Trent University, Brackenhurst Campus, Nottinghamshire, NG25 0QF, UK*

*Corresponding authors: gang.pan@ntu.ac.uk (G.P.); t.lyu@cranfield.ac.uk (T.L.)

The SI has 3 pages, which includes 4 figures.

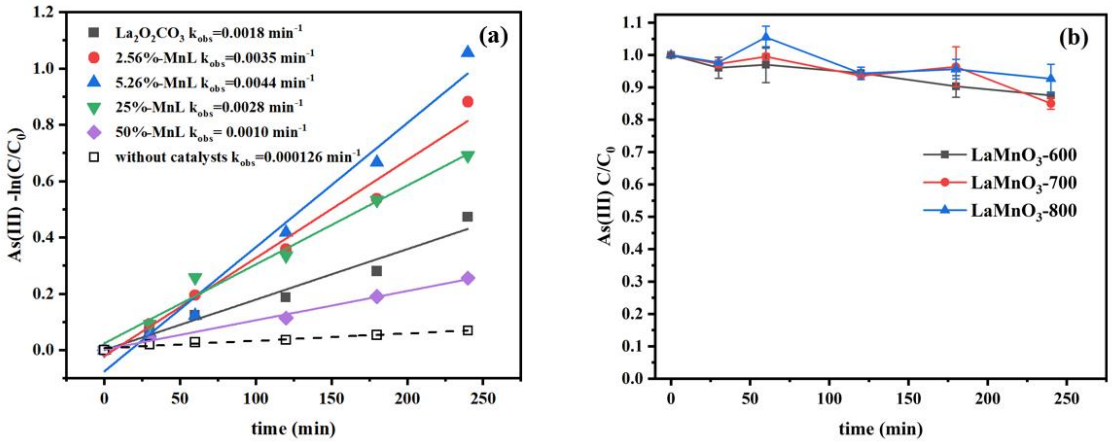

Fig. S1. (a) Pseudo-first order plots for As(III) oxidation in the MnL/H_2O_2 system, and (b) the oxidation efficiency of As(III) in $LaMnO_3$/H_2O_2 -coupled system with the $LaMnO_3$ synthesized at 600 ℃, 700 ℃, and 800 ℃.

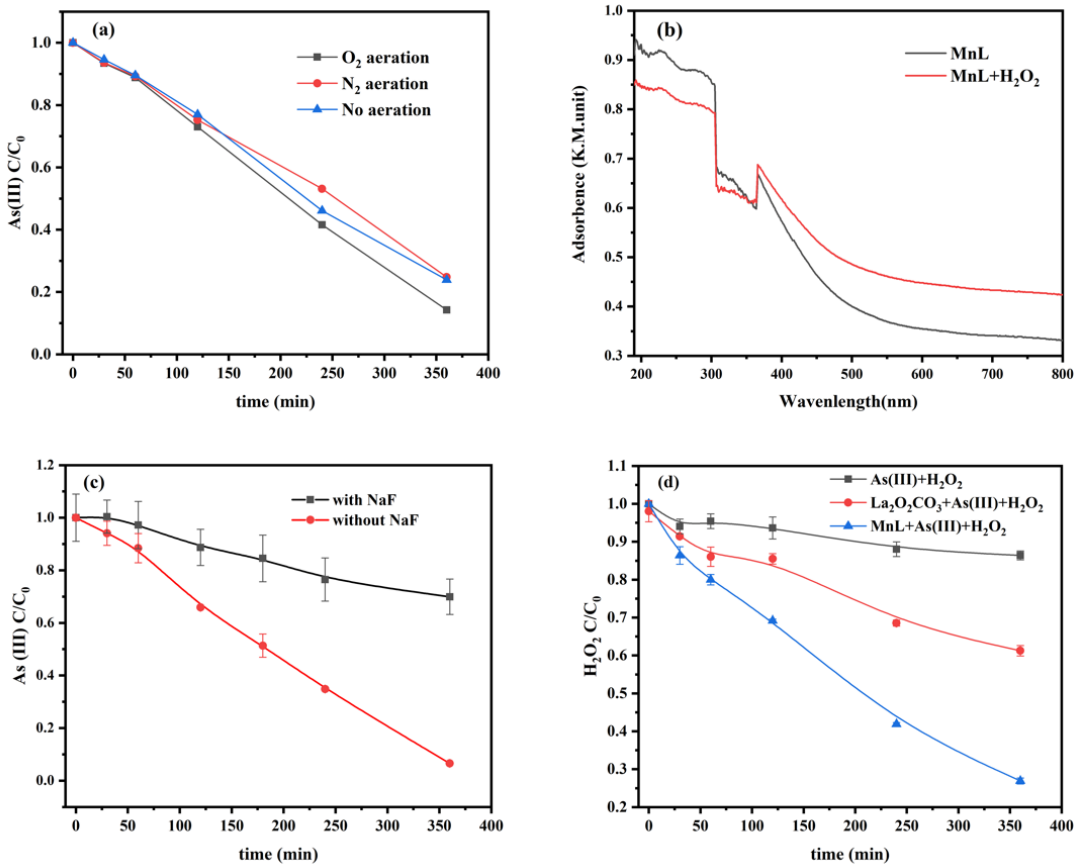

Fig. S2. (a) The effect of dissolved oxygen on As(III) oxidation in MnL/H_2O_2 system, (b) diffuse-reflectance UV-visible spectra (DR-UVS) of MnL in the presence and absence of H_2O_2, (c) the effect of NaF on As(III) oxidation in MnL/H_2O_2 system, and (d) the evolution of H_2O_2 during As(III) removal by MnL or $La_2O_2CO_3$/H_2O_2.

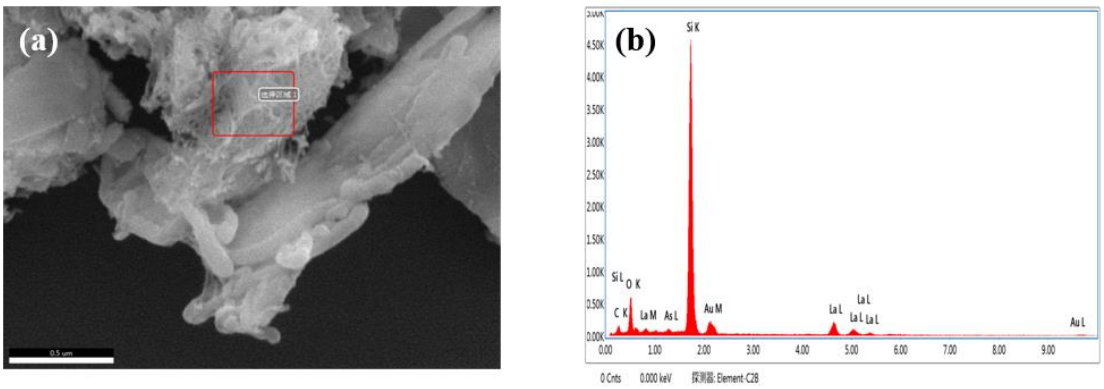

Fig. S3. (a) ESEM image and (b) EDS spectrum of MnL after As(III) oxidation.

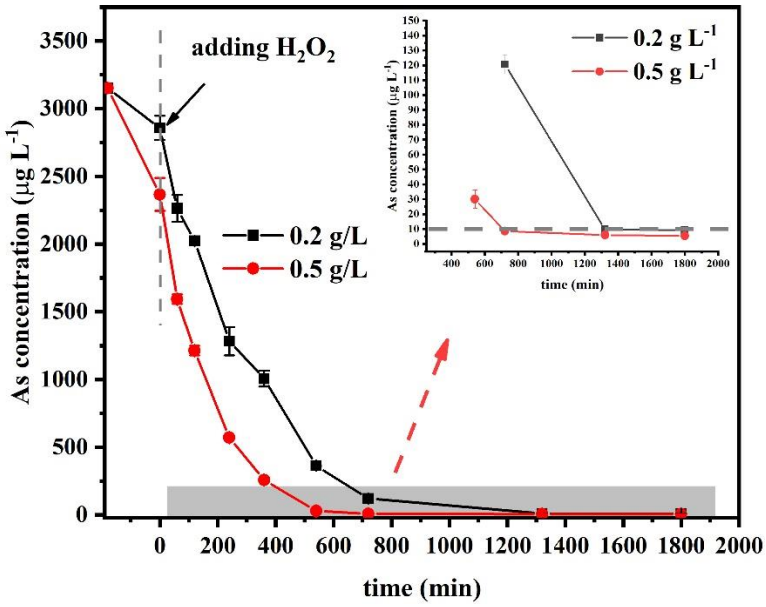

Fig. S4. Remnant As(III) in the MnL/H_2O_2 system with initial As(III) concentration of 3.15 mg L^{-1}.